Equations of State for Cu, Ag, and Au for Wide Ranges in Temperature and Pressure up to 500 GPa and Above

W. B. Holzapfel,[a] M. Hartwig, and W. Sievers
FB 6-Physik, Universität Paderborn, D-33095 Paderborn, Germany

(Received 8 September 2000; accepted 23 February 2001)

New constraints on the volume dependence of the Grüneisen parameter ($\gamma(V)$) are derived from a comparison of earlier shock wave data with more recent ultrasonic data for the bulk modulus K_0 and its pressure derivative K_0' in the frame of a rigorous Mie–Grüneisen model. This model uses a specially ''Modified pseudo-Debye–Einstein model'' for an accurate representation of the thermal energy and pressure. Within this framework, previous discrepancies between shock wave and static data concerning the equations of state for various reference materials (like Cu, Ag, and Au) are resolved, the corresponding pressure scale is refined, and the uncertainties in this scale are estimated.

Key words: Ag; anharmonicity; Au; Cu; equation of state; Grüneisen parameters; pressure scale; shock wave measurements; ultrasonic measurements.

Contents

List of Tables

List of Figures

[a]Electronic mail: holzapfel@physik.uni-paderborn.de

1. Introduction

One basic problem in solid state physics, geosciences, and even in planetology, is the precise thermodynamic characterization of the materials present in objects. A first step in this direction involves equations of state (EOS), most commonly in the form of a pressure–volume–temperature (pVT) relation. More generally, adiabatic pressure–volume–entropy (pVS) relations or caloric data for the internal energy, $U=U(p,T)$, are needed also in many cases. It is clear from basic thermodynamics that two of these relations,[1–3] like the ''thermal EOS'' $V=V(p,T)$, and the ''caloric EOS'' $U=U(p,T)$, determine completely the corresponding thermodynamic potentials, i.e., the internal energy $U=U(S,T)$, the (Helmholtz) free energy $F=F(V,T)$, the Gibbs potential $G=G(p,T)$, and the enthalpy $H=H(p,S)$ with respect to their ''canonic'' thermodynamic state variables given here in brackets.

The general problems involved in experimental determinations of EOS were reviewed recently.[4,5] It should be recalled here that various more or less semiempirical forms exist for the analytical representation of isotherms $V=V_T(p)$, or adiabats $V=V_S(p)$ and for the inverted forms $p=p_T(V)$ or $p=p_S(V)$. For the representation of shock wave results, special forms for Hugoniot data $p=p_H(V)$ have been derived.

For the complete description of the corresponding $p(V,T)$ or $p(V,S)$ surfaces, T or S dependent parameters like the isothermal bulk modulus $K_T=-V\cdot\partial p/\partial V|_T$, and its isothermal pressure derivatives, like $K_T'=\partial K/\partial p|_T=-\partial \ln K/\partial \ln V|_T$ and $K_T''=\partial^2 K/\partial p^2|_T=-(1/K_T)\cdot\partial K_T'/\partial \ln V|_T$, or the corresponding adiabatic quantities K_S, K_S', and K_S'' are commonly used. However, extrapolations of the resulting relations beyond the range of experimental data are usually dangerous, if the relations are not based on rigorous theoretical models.

Therefore, rigorous models for the ''cold'' EOS $p_c(V)$, related to the ground state energy of the solid $E_c(V)$, are commonly established, in a first step. In the second step some models are used for the thermal pressure[5–9]

$$p_{th}(V,T)=p(V,T)-p_c(V)=\gamma_{tb}(V,T)\cdot U_{th}(V,T)/V \tag{1}$$

to relate p_{th} to the thermal energy, U_{th}, by the use of a ''thermobaric'' Grüneisen parameter, γ_{tb}, defined by this relation. In the simplest case, usually called ''Mie–Grüneisen solid,'' it is assumed that $U_{th}=\theta\cdot u(\tau)$ with $\tau=T/\theta$. The volume dependence of U_{th} is represented only through the characteristic temperature $\theta(V)$ with its Mie–Grüneisen parameter

$$\gamma_\theta(V)=-d\ln\theta/d\ln V, \tag{2}$$

which is equal to γ_{tb} within the Mie–Grüneisen approximation.

So far, the functional form of $u(\tau)$ is completely free and the use of a Debye model for $u(\tau)$ involves rather rigorous assumptions, which can be avoided by far more flexible pseudo-Debye models.[7]

On the level of a rigorous Mie–Grüneisen approach with a pseudo-Debye model for the lattice heat capacity, one can determine the thermal phonon energy and entropy, the functional form for $u(\tau)$, and the value for θ at ambient pressure θ_0 from data for the heat capacity at ambient pressure $C_{p0}(T)$ or $C_{v0}(T)$. Only the volume dependence of the Grüneisen parameter $\gamma_\theta(V)$ remains to be determined.

The thermodynamic definition of the Grüneisen parameter

$$\gamma_{th}(V,T)=\alpha\cdot K_T\cdot V/C_V=\alpha\cdot K_S\cdot V/C_p, \tag{3}$$

on the other hand, relates the thermal volume expansion coefficient α, the bulk modulus K_T or K_S, the (specific) volume

V, and the (specific) heat capacity C_V or C_p to each other in such a way that an almost temperature independent ratio $\gamma_{\rm th}$ is obtained. From microscopic models, some temperature dependence of this $\gamma_{\rm th}$ can result from a dispersion of the ''mode Grüneisen parameters'' $\gamma_{i,k} = -d\ln \nu_{i,k}/d\ln V$, whereby i and k denote the different branches i and vectors k of the phonon dispersion curves.[9]

This temperature dependence of $\gamma_{\rm th}$ usually leads only to minor modifications of the thermal pressure $p_{\rm th}(V,T)$ at low temperatures ($T \ll \theta$), which can be neglected in the following discussion. At high temperatures ($T > \theta$) on the other hand, intrinsic anharmonicities[7,10,11] lead to a temperature dependence of $\gamma_{\rm th}$, which can be taken into account in first order with an anharmonicity parameter A_a and with $\delta_A = -dA_a/d\ln V$ in the forms

$$U_{\rm th} = 3Nk\theta(V)\cdot u(\tau)\cdot(1 + A_a\cdot(2\tau\cdot u'(\tau) - u(\tau))$$

and

$$\gamma_{\rm th} = \gamma_\theta\cdot(1 - 2\delta_A\cdot u(\tau)). \tag{4}$$

The usual Mie–Grüneisen approximation, however, corresponds to $\partial\gamma_{\rm th}/\partial T|_V = 0$ or $\delta_A = 0$ with a single $\gamma = \gamma_{\rm th} = \gamma_{\rm tb} = \gamma_\theta$. Later discussions of the experimental data for Cu, Ag, and Au will show that the EOS data are fitted reasonably within this simple Mie–Grüneisen approximation only at moderate temperatures, but anharmonic contributions with $\delta_A \neq 0$ are required for an accurate representation of the EOS data at higher temperatures ($T > \theta$).

2. Constraints on $\gamma(V)$

For a decision about the most reasonable form for $\gamma(V)$ one has to consider in detail the available theoretical and experimental constraints. First, and in general, accurate experimental data for γ_0, the value for ambient conditions, can be found in the literature[12] or by the use of more recent data for α_0, K_0, V_0, and C_{v0}. Second, in a recent discussion of the EOS data for Cu it was also shown[5] that data on the temperature dependence of the isothermal bulk modulus at ambient pressure $K_0(T)$ can be used to estimate the normalized volume derivative of γ at ambient conditions, $\Gamma_{\gamma 0} = \partial\ln\gamma/\partial\ln V|_{T,p=0}$, with an uncertainty of typically 20%.

A third constraint is given usually by γ_∞, the value of γ at very strong compression. Theoretical considerations of a lattice of positive ions in a degenerate electron gas[13–17] predict a value of $\gamma_\infty = 1/2$, whereas the value for a degenerate electron gas is $\gamma_\infty = 2/3$. Often this last value is favored for solids[8,18–27] probably due to the fact that the linear temperature dependence of the electronic specific heat of the degenerate free electron gas will dominate over the phonon contribution when the Debye temperature is increased sufficiently. With reasonable values for the initial Fermi energy, for the initial Debye temperature, for the Grüneisen parameter, and for the initial reference temperature, $T_R (< 1000\,{\rm K})$, one can estimate that this crossover occurs at more than tenfold compression. Within a rigorous Mie–Grüneisen model the electronic $\gamma_\infty = 2/3$ should then be adopted for this range.

In addition to these three constraints on $\gamma(V)$, shock wave data are often used with ''iterative procedures''[6,8,22–27] to obtain a best fit of both the cold EOS and some empirical form for $\gamma(V)$ with respect to the Hugoniot pressure of the shock wave data.

However, instead of going through an iterative procedure, a further constraint for $\gamma(V)$ can be derived more directly from shock wave data for ''regular'' solids (i.e., for solids without any structural phase transitions or electronic transitions in the region of interest). In fact, it is well known[6,28] that many ''regular'' solids show regular linear relations between shock wave velocities u_s and particle velocities u_p with the implication[1,6,29–32] that the corresponding Hugoniot pressure p_H is represented with respect to the relative volume $v = V/V_0$ by the relation (previously[5] also named MS2)

$$p_H = K_{H0}\cdot(1-v)/(1 - c\cdot(1-v))^2, \tag{5}$$

with K_{H0} and c as free parameters determined, respectively, from the initial value and the slope of the linear $u_s - u_p$ relation. If the linear $u_s - u_p$ relation holds perfectly down to ambient pressure, the parameters K_{H0} and $K'_{H0} = 4\cdot c - 1$ could be related to the isothermal values K_{T0} and K'_{T0}. However, small initial nonlinearities in the $u_s - u_p$ relations[28] together with problems related to the Hugoniot elastic limit at moderate shock compressions[33] restrict the precision in this extrapolation at low pressures.

Nevertheless, linear extrapolations of the $u_s - u_p$ relations towards strong compression point to another special feature of Eq. (5). At the critical volume V_c or at the critical volume ratio $v_c = V_c/V_0 = (c-1)/c$, the Hugoniot pressure $p_H(V_c) \Rightarrow \infty$ diverges.[6] This divergence implies that strong shocks in this region lead only to stronger heating and to a divergence of the thermal pressure $p_{\rm th}(V_c)$, whereas the cold pressure for this critical compression remains finite.

The well-known Hugoniot relations between the measured velocities $u_s - u_p$ and the deduced values for the shock pressure (p_H) on the one hand and for the internal energy (U_H) on the other hand both at the final state volume (V) can then be used[1,6,31,32] with

$$p_H = p_c(V) + p_{\rm th}(V,T), \quad U_H(V,T) = E_c(V) + U_{\rm th}(V,T),$$

and

$$p_{\rm th} = (\gamma/V)\cdot U_{\rm th}$$

to derive a rigorous relation for γ_H

$$\gamma_H(V) = V\cdot\frac{p_H(V) - p_c(V)}{U_H(V) - E_c(V)}. \tag{6}$$

In the limit of $V \to V_c$, as discussed before, p_H and U_H dominate over p_c and E_c, respectively, and one obtains[6]

$$\gamma_c = 2\cdot(c-1) = 2\cdot v_c/(1-v_c). \tag{7}$$

In other words, independent of the special form for $p_c(V)$, linear $u_s - u_p$ relations give one additional constraint for γ by the value γ_c at the critical volume V_c. One may object that this value of γ_c is obtained by extrapolation. However, this extrapolation is not so critical, since the experimental values

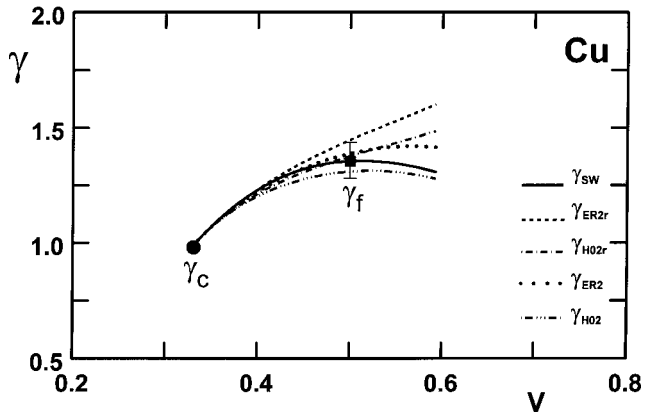

FIG. 1. Determination of γ_f from shock wave data for Cu. For details see text.

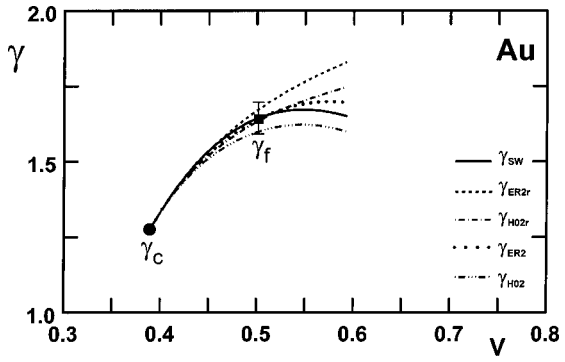

FIG. 3. Determination of γ_f from shock wave data for Au. For details see text.

for the volume in the shocked state already come close to V_c and the extrapolation in $\gamma \rightarrow \gamma_c$ is rather smooth in Eq. (6). To gain more insight into the approach of $\gamma \rightarrow \gamma_c$, one can also calculate directly the variation of $\gamma(V)$ from the form Eq. (6) with $U_H = (V_0 - V) \cdot p_H/2$ and $p_H(V)$ from Eq. (5) together with different forms for $p_c(V)$ and $E_c(V)$. For the sake of simplicity, just two similar forms for $p_c(V)$ are used in the further discussion.

The form

$$p = 3 \cdot K_0 \cdot (1-x) \cdot x^{-n} \cdot \exp(c_{2n} \cdot (1-x)) \qquad (8)$$

with $x = v^{1/3} = (V/V_0)^{1/3}$ and $c_{2n} = (3/2) \cdot K_0' - n + 1/2$ can be considered to result from a nearest neighbor interaction by an ''effective'' Rydberg potential, when $n = 2$ is selected, and therefore it is called ER2 for $n = 2$. Previously, this form with $n = 2$ was called ''universal'' EOS[34] also somewhat more systematically MV2, when it was shown[35] that only the exponent $n = 5$ results in the correct asymptotic behavior at very strong compression. With $n = 5$ this form was named H02. In both cases, $E_c(V)$ can be obtained by integrating $p_c(v)dv$. The results with respect to the evaluation of the shock wave data for Cu, Ag, and Au are shown in Figs. 1–3 for different parameter sets. First of all, the parameter c was derived from shock wave data,[28] discarding data for $v < 0.7$, which could be effected by melting and electronic excitations.[6] In this way the average values for c with estimated errors were obtained, but only the corresponding values $K_{H0}' = 4 \cdot c - 1$ are given in Table 1, to allow for a direct comparison with values for the isothermal K_0' as most reasonable average values, which were derived from ultrasonic data.[7,35–47] For the curves labeled ER2 and H02, respectively, equal values for the isothermal and Hugoniot values, $K_0 = K_{H0}$, in Eqs. (6) and (8) were used. Due to the slight curvature of the $u_s - u_p$ relations near $v \Rightarrow 1$ and the correspondingly different values for K_{H0} from linear high-pressure extrapolations, an upper estimate for the ratio $r = K_{H0}/K_0 = 1.08$ was introduced for the curves ER2r and H02r in all three cases. Figures 1–3 show clearly that the critical values γ_c represent lower limits and more reliable fiducial values γ_f may be obtained at somewhat larger vol-

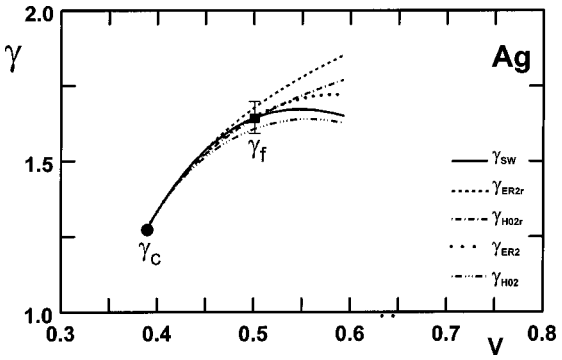

FIG. 2. Determination of γ_f from shock wave data for Ag. For details see text.

TABLE 1. Primary data for the determination of the present EOS forms. These data include estimated uncertainties for the ''best'' values from the literature.

$T_R = 300$ K	Cu	Ag	Au	Ref.
V_{0R}/nm^3	0.011815(1)	0.017057(1)	0.016959(1)	a
K_{0R}/GPa	133.2(2)	101.0(2)	166.7(2)	b
K_{0R}'	5.40(15)	6.15(15)	6.20(15)	c
K_{H0}'	5.0(2)	5.6(3)	5.6(3)	d
θ_{D0}/K	342(2)	228(3)	165(3)	e
γ_0	2.00(10)	2.45(10)	3.05(10)	f
$\Gamma_{\gamma 0}$	1.40(5)	1.70(5)	2.40(5)	g
f_1	0.54	0.50	0.50	h
f_2	0.86	0.90	1.10	h
A_a	0.005(2)	0.001(2)	0.001(2)	h
δ_A	0.030(5)	0.030(1)	0.032(3)	i
θ_{Dav}/θ_{D0}	1.12(5)	1.13(5)	1.29(5)	h

[a]See Wyckhoff.[54]
[b]Ultrasonic data, see Refs. 36–45.
[c]Ultrasonic data, see Refs. 43–45.
[d]Shock wave data, see Refs. 23, 28, 58–60, 62, 64, 67, 68.
[e]Gschneidner.[12]
[f]From Refs. 12, 23, 43 and reevaluation with additional data for V_0, K_0, α_0, C_p from Refs. 55–57.
[g]Present fit of $V_0(T)$ data (Refs. 55 and 56) and $K_0(T)$ data (Refs. 39, 44, 45) with MoDE2 ansatz.
[h]Present fit of $C_p(T)$ data (Refs. 56 and 57) with MoDE2 ansatz.
[i]From a recent fit[11] of $\gamma_{th0}(T)$ data with MoDE2-ansatz.

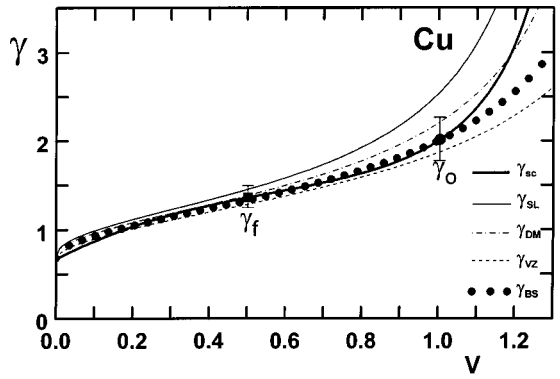

FIG. 4. Comparison of different forms for $\gamma(v)$ of Cu. For details see text.

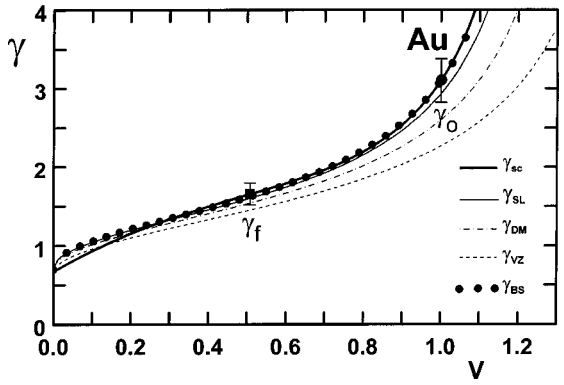

FIG. 6. Comparison of different forms for $\gamma(v)$ of Au. For details see text.

umes. Best estimates of $\gamma_H(v_f)$ for $v_f<0.5$ are shown in Figs. 1–3, whereby a polynomial expansion with respect to $\delta=(v_f/v_c)-1$ in the form

$$\gamma_H(\delta)=\frac{2\cdot v_c}{1-v_c}\cdot\left(1+\frac{\delta}{1-v_c}(1-a\cdot\delta)^2\right) \tag{9}$$

with $a=38(2)(1-v_c)^2v_c^2$ gives reasonable values for all three cases. The total uncertainty in $\gamma_H(v_f)$ can be estimated by upper and lower bounds on v_c in each case together with upper and lower bounds for a with its prefactor 38(2). The best fiducial value γ_f may be obtained now for $\delta\approx0.15$ or for $v_f=0.5$ just at the upper end of the experimental region of the shock wave data, where electronic excitations are still negligible and where the divergence of the different curves is still rather small. The total uncertainty in this best fiducial value γ_f at $v_f=0.5$ is then expected to be less than 10% as illustrated in Figs. 1–3 by the corresponding error bars.

With these constraints on $\gamma(V)$, now one can test various analytical forms or ''theoretical'' results present in the literature in comparison to some form, which appears to be most appropriate for the tabulation of EOS data for reference materials.

3. The Volume Dependence of γ

Many earlier discussions on the volume dependence of γ were related to the Debye approximation for the phonon dispersions.[1,6,31,48–51] With different assumptions about the volume dependence of Poisson's ratio and with a ''free volume theory,'' respectively, three different forms for γ were derived by Slater,[48] Dugdale-MacDonald,[49] and Vashchenko-Zubarev.[50] The original form from Slater

$$\gamma_{\rm SL}=K'(v)/2-1/6 \tag{10}$$

was modified in the later approaches by the subtraction of the term

$$\varepsilon=m\cdot(K-K'\cdot p)/(3\cdot K-2\cdot m\cdot p) \tag{11}$$

with[49] $m=1$ or[50,51] $m=2$, respectively. Since no universal value of m can fit the experimental data for γ at ambient conditions,[6,43] one may consider m as an adjustable parameter with respect to the value of γ_0. This kind of generalized Slater form

$$\gamma_{\rm BS}=K'/2-1/6-m\cdot(K-K'\cdot p)/(3\cdot K-2\cdot m\cdot p), \tag{12}$$

with $m=3\cdot K_0'/2-1/2-3\cdot\gamma_0$ is labeled in Figs. 4–6 with $\gamma_{\rm BS}$, since it had been shown that this form with noninteger value for m can be derived from central force models, when correlations of the motions for neighboring atoms are taken into account.[52,53] In fact, this Barton–Stacey form $\gamma_{\rm BS}$ shows some interesting features, which are illustrated in Figs. 4–6, where the other forms for $m=0$, 1, and 2 with the labels SL, DM, and VZ, respectively, are also presented for comparison.

All these forms can be derived for strong compressions only if the corresponding $p(v)$ relation, with its derivatives $K(v)$ and $K'(v)$, is also known. In Figs. 4–6 only the *interpolating* EOS form AP2 for (regular) solids under strong compression[5] is used with the appropriate parameters V_0, K_0,K_0', and Z for Cu, Ag, and Au from Table 1, recalling that this form AP2 is given[5] by

$$p=3\cdot K_0\cdot\frac{1-x}{x^{-5}}\cdot e^{c_0(1-x)}\cdot(1+c_2\cdot x\cdot(1-x)), \tag{13}$$

with

$$x=(V/V_0)^{1/3}\quad c_2=(3/2)\cdot(K_0'-3)-c_0$$

$$c_0=-\ln(3\cdot K_0/p_{\rm FG0})$$

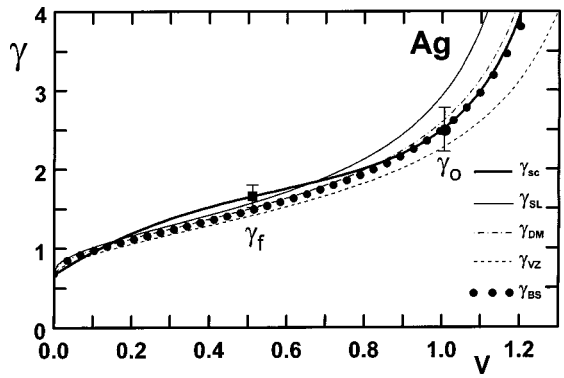

FIG. 5. Comparison of different forms for $\gamma(v)$ of Ag. For details see text.

TABLE 2. Fiducial values γ_f derived from the K'_{H0} values of Table 1 and comparison with calculated values for γ_{BSf} and $\Gamma_{\gamma BS0}$ as discussed in the text. Additional secondary parameters, V_r, v_d, A, B, $\Delta\gamma_\infty$, and θ_{Dav}/θ_{D0} are given for a convenient representation of the EOS data.

$T_R = 300$ K	Cu	Ag	Au
$\Gamma_{\gamma BS0}$	1.07(14)	1.46(13)	2.24(8)
γ_{BSf}	1.36(3)	1.57(3)	1.67(3)
γ_f	1.36(13)	1.64(16)	1.64(16)
V_r	1.41(1)	1.35(1)	1.35(1)
v_d	1.42	1.32	1.31
A	0.50	0.43	0.70
B	0.62	1.12	0.78
$\Delta\gamma_\infty$	0.51	0.78	0.65

and

$$p_{FG0} = a_{FG} \cdot (Z/V_0)^{5/3}.$$

With respect to the previously used form H02 given by Eq. (8), the form AP2 is modified in such a way that the correct Thomas–Fermi limit is obtained at very strong compressions. For this purpose, c_0 involves the effective Fermi gas pressure for ambient conditions p_{FG0}, which contains the universal parameter $a_{FG} = 23.37\ \text{MPa nm}^5$ for the Fermi gas.

With this form AP2 as well as for the form H02, γ_{BS} approaches for any value of m the same value $\gamma_\infty = 2/3$ at very strong compression. However, the adjustable parameter m effects the (normallized) slope of γ at ambient conditions by its correlation to the experimental value for γ_0, and one obtains

$$\Gamma_{\gamma BS0} = (-3 \cdot K_0 \cdot K_0'' - (3 \cdot K_0' - 1 - 6 \cdot \gamma_0) \times (2 \cdot \gamma_0 + 1/3))/(6 \cdot \gamma_0). \quad (14)$$

The experimental values for the slope $\Gamma_{\gamma 0}$ at $v = 1$ from Table 1 are represented in Figs. 4–6 by the slopes of the curves labeled γ_{SC}, which include all the experimental and theoretical constraints, to be discussed later, and which are considered to represent the ''best fit'' to all the available data. As one can see in Figs. 4–6 the slopes of γ_{BS} at $v = 1$ for the EOS form AP2 come very close to the experimental data in the cases of Ag and Au. In the case of Cu, Fig. 4 shows a significant difference in the slope of the curve γ_{BS} with respect to γ_{SC} at $v = 1$. The other Slater type forms $\gamma_{SL}, \gamma_{DM}, \gamma_{VZ}$ show their specific deviations from the experimental value at ambient conditions but converge all to the same value at $v = 0$, if the same EOS form AP2 is used in all three cases. However, the constraint on $\Gamma_{\gamma 0}$ incorporated into γ_{BS} may be regarded as somewhat rigorous and reasonable only for ''reasonable'' EOS forms. On the other hand, one can consider some of this discrepancy with respect to γ_{BS} in the case of Cu also as a hint, which indicates that the experimental value for $\Gamma_{\gamma 0}$ given in Table 1 may be slightly too large in this case. On the other hand, the estimates for $\Gamma_{\gamma BS0}$ based on the slopes of γ_{BS} given in Table 2 represent only the average values derived from the forms AP2 and H02 with an ''error estimate'' giving the maximum deviation from these average values and not a true error estimate. A comparison with the experimental data in Table 1 shows that only the value 1.07 for Cu in Table 2 is significantly smaller than the lower limit for the experimental value. However, the total uncertainties of the ''experimental'' values for $\Gamma_{\gamma 0}$ in Table 1 are also not well known, since these values are derived by best fits of $V_0(T)$, $K_0(T)$, and $K_0'(T)$ under the assumption that the extended Mie–Grüneisen model with A_a and $\delta_A \neq 0$, discussed in detail later, is a good approximation.

On the other hand, one can notice in Figs. 4 and 6 that γ_{BS} for AP2 passes almost exactly through the reference value γ_f, but in the case of Ag (Fig. 5), one can see a small difference between γ_{BS} and γ_f. These differences between γ_{SC} and γ_{BS} (based on AP2) could either be used as estimates for the uncertainties still involved in the evaluation of $\gamma(v)$, or they can be used to define a correction term $\varepsilon(m,p)$ for γ_{BS} for instance in the form of a series expansion of $\varepsilon(m,p)$ around $v = 0$ or 1 using the previous constraints for γ_0, $\Gamma_{\gamma 0}$, γ_∞, and γ_f. However, this approach leads to unreasonable variations, and it is clear that these unreasonable anomalies can be traced back to the fact that all these forms for any m take into account primarily mode Grüneisen parameters for the long wavelength phonons, which must diverge for $v \to v_r$ like $K'(v)$, whereby v_r represents the extrapolated ''rupture volume'' for which $K(v_r) = 0$. In fact, all the other mode Grüneisen parameters may behave more regularly near v_r, and therefore the factor 1/2 in front of $K'(v)$ could be adjusted to a smaller value to give a smoother variation in $\varepsilon(v)$. Tests along this line lead to the observation that such a prefactor for $K'(v)$ becomes quite small, equal to 0.15 for Cu and 0.08 for Au, or even negative, depending on the other constraints. This means that the form of $K'(v)$ seems to imply unreasonable constraints for $\gamma(v)$. If one wants to keep in the expansion of $\gamma(v)$ for $v \to v_r$ at least one term which qualitatively reproduces the divergence of $K'(v)$ at $v \to v_r$, one may use a simpler form with prefixed v_r and the adjustable parameters γ_∞, γ_0, b_1, and b_2 as given by the relation

$$\gamma_{VR} = \gamma_\infty + b_1 \cdot v/(v_r - v) + b_2 \cdot v + b_3 \cdot v \cdot (1 - v), \quad (15)$$

with

$$b_1 = (4 \cdot \gamma_f - \gamma_\infty - 3 \cdot \gamma_0 + \gamma_0 \cdot \Gamma_{\gamma 0})(2 \cdot v_r - 1)(v_r - 1)^2,$$

$$b_2 = \gamma_0 - \gamma_\infty - b_1/(v_r - 1),$$

and

$$b_3 = \gamma_0 - \gamma_\infty - \gamma_0 \cdot \Gamma_{\gamma 0} + b_1/(v_r - 1)^2.$$

A similar form with $b_3 = 0$ and a free parameter v_a instead of the prefixed rupture volume v_r can be found in the literature,[15] however, without the linear term in v. With the linear term and the previous constraints one obtains the following form:

$$\gamma_{VA} = \gamma_\infty + b_a \cdot v/(v_a - v) + (\gamma_0 - \gamma_\infty - b_a/(v_a - 1)) \cdot v, \quad (16)$$

with

$$v_a = 1 + (\gamma_0 + \gamma_\infty - 2\cdot\gamma_f)/(4\cdot\gamma_f - \gamma_\infty - \gamma_0\cdot(3-\Gamma_{\gamma 0})),$$

and

$$b_a = (\gamma_0\cdot\Gamma_{\gamma 0} + \gamma_\infty - \gamma_0)\cdot(v_a - 1)^2.$$

In fact, the behavior of this form is very similar to another recently considered form[24] from the point of view that the fitted value of v_a may fall into the range $0 < v_a < 1$ with the effect that γ_{VA} may show unreasonable divergencies in the ''experimental'' region. Therefore, γ_{VA} is not taken into account any further.

Some other forms of $\gamma(v)$ for applications over extended pressure and temperature ranges including both the solid and the fluid phases avoid the singularity expected in the region $v > 1$, where the solids become unstable, but keep a maximum at the corresponding volume. One of these forms[24]

$$\gamma_{BL} = \gamma_\infty + (\gamma_0 - \gamma_\infty)\cdot v\cdot(1 + v_{BL}^2)/(v^2 + v_{BL}^2)$$

allows one to adjust only v_{BL}^2 to one additional constraint, either to γ_f or to the slope $\Gamma_{\gamma 0}$.

Some other common forms[23] like

$$\gamma_{AB} = \gamma_\infty + (\gamma_0 - \gamma_\infty)\cdot v^q$$

or[17,19]

$$\gamma_{TL} = \gamma_0\cdot v + \gamma_\infty\cdot(1-v)^n$$

will not be discussed in further detail here, since these forms appear to be more suitable for cases where the experimental information is more limited either with respect to $\Gamma_{\gamma 0}$, γ_f, or γ_∞ (for instance due to phase transitions).

However, one other form seems to be interesting, since it follows within the region $v > 1/2$ the variation represented by γ_{VR}, very closely, but analytically it is much simpler

$$\gamma_{mc} = A/(v_d - v) + B, \tag{17}$$

with

$$A = (\gamma_0 - B)\cdot(v_d - 1),$$

$$B = \gamma_0\cdot(1 - \Gamma_{\gamma 0}\cdot(v_d - 1)),$$

$$v_d = 1 + \frac{\gamma_0 - \gamma_f}{\gamma_0\cdot\Gamma_{\gamma 0} - 2\cdot(\gamma_0 - \gamma_f)},$$

and

$$\Delta\gamma_\infty = A/v_d + B - \gamma_\infty,$$

which is significantly different from zero for Cu, Ag, and Au as shown in Table 2.

Therefore, this form is reasonable only for moderate compression and only for $v_d > 1$, or in other terms for $\Gamma_{\gamma 0} > 2\cdot(1 - \gamma_f/\gamma_0)$, which holds at least for Cu, Ag, and Au. This form γ_{mc} can easily be integrated in closed form to give the very useful relation

$$\ln\left(\frac{\theta_{mc}}{\theta_0}\right) = \left(\frac{A}{v_d}\right)\cdot\ln\left(\frac{v_d - v}{v_d - 1}\right) - (\gamma_\infty + \Delta\gamma_\infty)\cdot\ln(v). \tag{18}$$

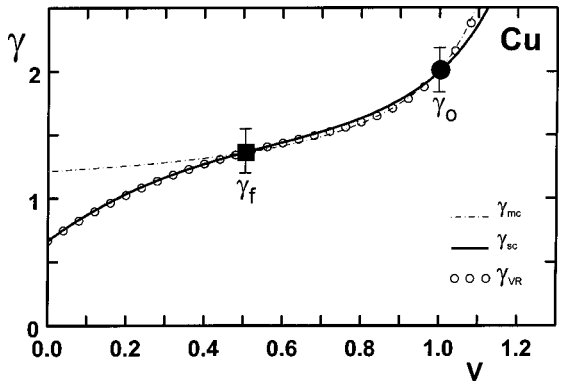

FIG. 7. Most likely variation of $\gamma(v)$ for Cu given by γ_{SC} with probable uncertainties. For comparison, γ_{mc}, as well as γ_{VR}, are also shown.

γ_{mc} can be extended also to strong compression by an additional term, which maintains all the previous constraints and adds a linear approach towards γ_∞

$$\gamma_{sc} = \gamma_{mc} + \Delta\gamma_\infty\cdot(2v-1)(1-v)^2, \tag{19}$$

with

$$\ln(\theta_{sc}/\theta_0) = \ln(\theta_{mc}/\theta_0) + \Delta\gamma_\infty \cdot(\ln(v) + (13 - 11\cdot v + 4\cdot v^2)(1-v)/6).$$

In fact, this form needs only experimental data and no extrapolation of any EOS as, for instance, all the forms related to Slater's approach and also γ_{VR}, which requires an extrapolation to obtain v_r. In any case, it is interesting to note that the input data K_0 and K_0' from Table 1 for Cu, Ag, and Au result with any of the EOS forms AP2, H02, and ER2 for v_r the values in Table 2, which are quite close to the values v_d derived from the independent input data γ_0, $\Gamma_{\gamma 0}$, and γ_f (based on c). For the practical use of Eqs. (18) or (19) Table 2 gives then the secondary parameters A, B, v_d, and $\Delta\gamma_\infty$.

4. Discussion of γ(V) for Cu, Ag, and Au

First of all, Figs. 7–9 illustrate that the forms γ_{mc}, γ_{sc}, and γ_{VR} represent very similar variations within the ''experi-

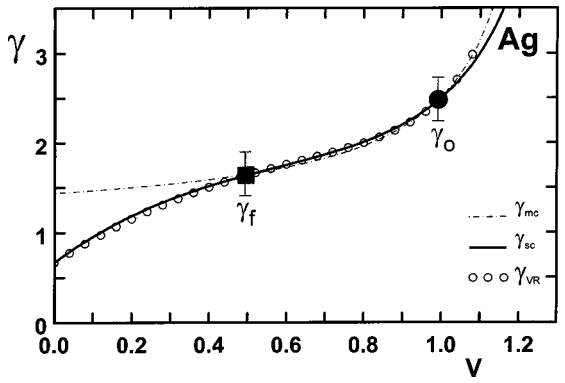

FIG. 8. Most likely variation of $\gamma(v)$ for Ag given by γ_{SC} with probable uncertainties. For comparison, γ_{mc}, as well as γ_{VR}, are also shown.

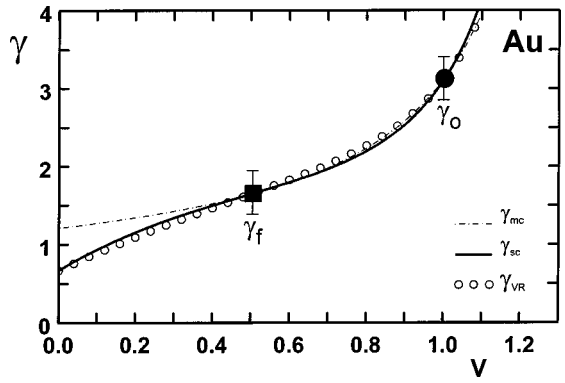

FIG. 9. Most likely variation of $\gamma(v)$ for Au given by γ_{SC} with probable uncertainties. For comparison, γ_{mc}, as well as γ_{VR}, are also shown.

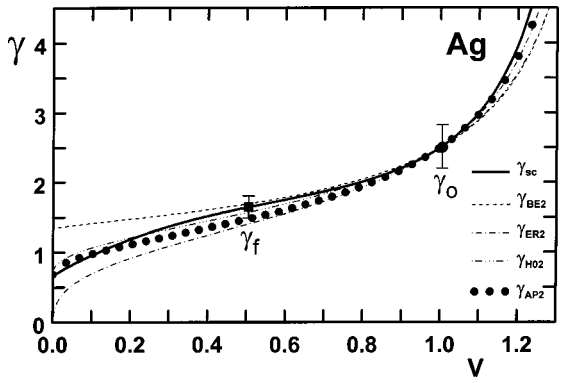

FIG. 11. Comparison of γ_{BS} values evaluated from different EOS forms discussed in the text with respect to the best fit γ_{SC} and its likely uncertainties for Ag.

mental'' region $0.5<v\leqslant 1$. Only for extrapolations to smaller values of v may one use γ_{sc} or γ_{VR}. Again, in this region, both of these forms result in very similar variations with respect to the estimated uncertainties. It should be noted, however, that γ_{sc} uses only the experimental input data from Table 1 and no extrapolated values like γ_{VR} with its predetermined value for the ''rupture volume'' v_r. Due to this fact, the curves γ_{sc} will be used from now on as ''best references'' together with the corresponding upper and lower limits denoted by error bars and derived from the upper and lower limits for γ_∞, γ_f, and γ_0, respectively. Thereby, the value for $\Gamma_{\gamma 0}$ was kept fixed, because the combined uncertainties of γ_f and γ_0 cover already the region of the additional uncertainty in $\Gamma_{\gamma 0}$. For the uncertainty of $\gamma_\infty \pm 1/6$ was used for the uncertainty to include on the one hand the lower limit 1/2 given at various places in the literature.[13–17] On the other hand, the upper limit 5/6 was selected somewhat arbitrarily to allow for a linear increase of γ with $x=v^{1/3}$ for $v\leqslant 0.1$, typical for all the Slater type curves and also derived in some theoretical studies.[17]

On the basis of this best estimate γ_{sc} with its ''experimental'' uncertainties (denoted by error bars in Figs. 10–12) one can see that the use of different EOS forms in the evaluation of the Barton–Stacey form γ_{BS} given by Eq. (12) leads to some interesting features. First of all, both the EOS forms AP2 and H02 give very similar curves and approach the expected value at very strong compression. Since these curves, like all the other Barton–Stacey curves, have been adjusted only to fit γ_0, small deviations in the initial slope $\Gamma_{\gamma 0}$ and with respect to the fixed point γ_f have to be expected. The second order Birch (BE2) and Vinet (ER2) type EOS forms,[5] on the other hand, lead to divergences under strong compression, which result in significant deviations from a reasonable variation already at moderate compression, especially in the case BE2 for Cu, Fig. 10.

This means, that the Barton–Stacey form gives some further support to the previous conclusion[5] that both these forms BE2 and ER2 as well as their higher order modifications are not suitable for extrapolations concerning the behavior of ''regular'' solids under strong compression.

Since the Barton–Stacey form uses as input parameters the temperature dependent values for $K_0(T)$, $K_0'(T)$, and $\gamma_0(T)$ [see Eq. (12)], one might expect that the resulting form $\gamma_{BS}(v)$ also depends on temperature, in contrast to the Mie–Grüneisen assumption $\partial\gamma/\partial T|_v=0$. To avoid this problem, one could argue that γ_{BS} should always be evaluated from the corresponding EOS form for the static lattice case. If one evaluates, however, the temperature dependence of

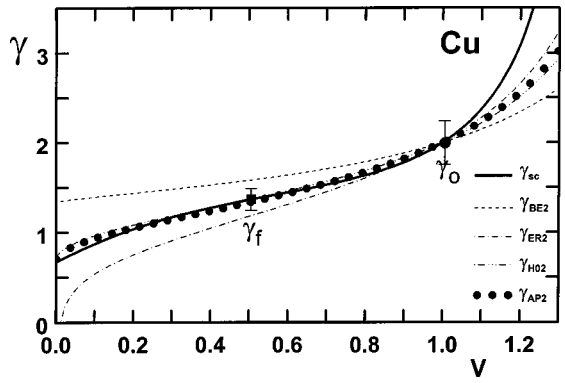

FIG. 10. Comparison of γ_{BS} values evaluated from different EOS forms discussed in the text with respect to the best fit γ_{SC} and its likely uncertainties for Cu.

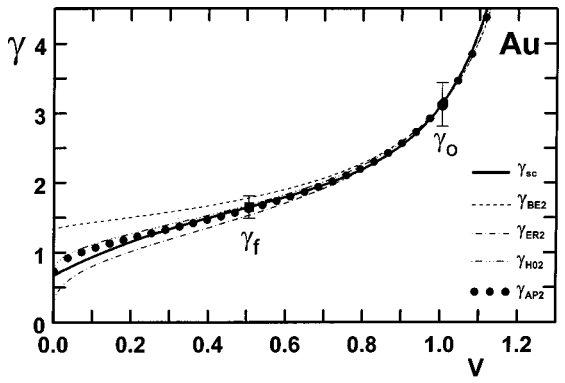

FIG. 12. Comparison of γ_{BS} values evaluated from different EOS forms discussed in the text with respect to the best fit γ_{SC} and its likely uncertainties for Au.

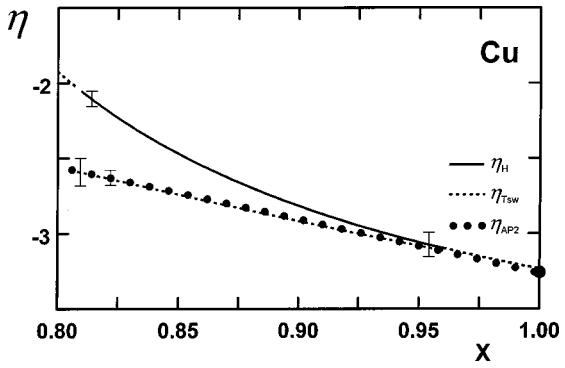

FIG. 13. APL scaling η_H, η_T, and η_{AP2} for Cu based on of the Hugoniot data p_H, the derived isothermal pressures p_T and the isothermal data p_{AP2}, respectively. The isothermal pressure for p_{AP2}, represents thereby the form AP2 with ultrasonic data for K_0 and K_0'. The isothermal value K_{T0} at ambient conditions is marked by the solid dot. The error limits for p_H and p_T are indicated by error bars and for p_{AP2} almost by the sizes of the dots, respectively.

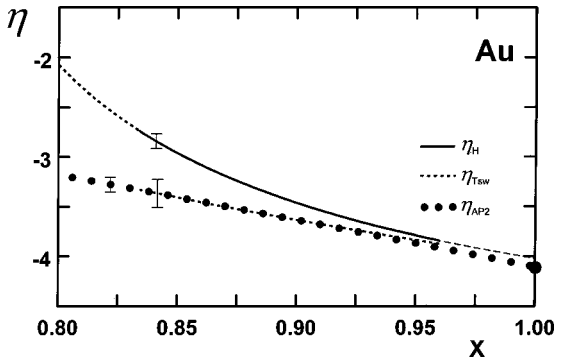

FIG. 15. APL scaling η_H, η_T, and η_{AP2} for Au based on of the Hugoniot data p_H, the derived isothermal pressures p_T, and the isothermal data p_{AP2}, respectively. The isothermal pressure for p_{AP2} represents thereby the form AP2 with ultrasonic data for K_0 and K_0'. The isothermal value K_{T_0} at ambient conditions is marked by the solid dot. The error limits for p_H and p_T are indicated by error bars and for p_{AP2} almost by the sizes of the dots, respectively.

γ_{BS} from different isotherms represented by the form AP2 with temperature dependent input parameters $V_0(T)$, $K_0(T)$, and $K_0'(T)$, one finds that the effects of temperature would be noticeable only when the accuracy for γ is better than 0.2% over the whole range of $0<v<1.05$.

A comparison of the original Hugoniot data $p_H(v)$ with different forms for the isotherms (at ambient temperature) can be performed now with the error estimates for both the original Hugoniot data[29,30,58–60,62–65,67–68] and the resulting uncertainties for the calculated isothermal values $p_T(v)$ as illustrated in the Figs. 13–15 for Cu, Ag, and Au, respectively, in the form of an APL-scaling, introduced earlier[5,33] to represent EOS data in such a way that a linear variation is obtained for ''simple'' solids and the approach toward the Fermi gas limit is shown by $\eta(0)=0$ with[69]

$$\eta=\ln(p/p_{FG})-\ln(1-x) \tag{20}$$

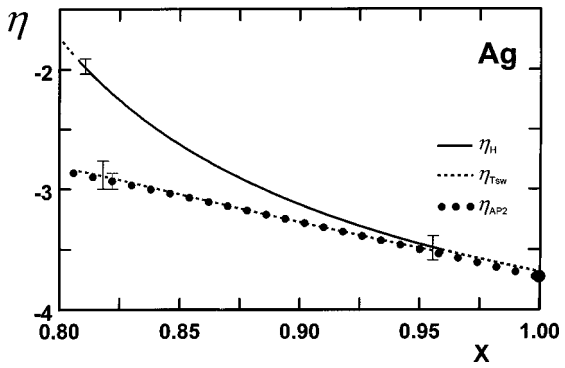

FIG. 14. APL scaling η_H, η_T, and η_{AP2} for Ag based on of the Hugoniot data p_H, the derived isothermal pressures p_T, and the isothermal data p_{AP2}, respectively. The isothermal pressure for p_{AP2} represents thereby the form AP2 with ultrasonic data for K_0 and K_0'. The isothermal value K_{T_0} at ambient conditions is marked by the solid dot. The error limits for p_H and p_T are indicated by error bars and for p_{AP2} almost by the sizes of the dots, respectively.

with $x=(V/V_0)^{1/3}$, $p_{FG}=p_{FG0}/x^5$, and p_{FG0} as given in Eq. (13). If one use p_{AP2} from Eq. (13) for p in this form, one obtains

$$\eta_{AP2}=-c_0\cdot x+\ln(1+c_2\cdot x\cdot(1-x)), \tag{21}$$

which gives just a linear variation for ''simple'' solids defined by $c_2=0$. Since $\Delta U_{th}=p_H\cdot\Delta V/2-\Delta E_c$ can be obtained from the Hugoniot data p_H and from $\Delta E_c=\int_{v_0}^{v}p_c(V)dV$, as discussed in Sec. 1, the use of the present best fits for γ_{sc} together with the estimated uncertainties results on the other hand in the curves labeled p_T, which represent the best estimates for the shock wave based ''experimental'' isotherms.

As seen in Figs. 13–15, the form AP2 with K_0 and K_0' from ultrasonic measurements near ambient conditions fits perfectly into the ''experimental'' region determined from the shock wave data. The other EOS forms included in the expanded views given in Figs. 16–18 show usually larger deviations from the best estimate p_T. The form BE2 shows a tendency to result in higher values (larger pressures) at strong compression, whereas ER2 shows in these cases the

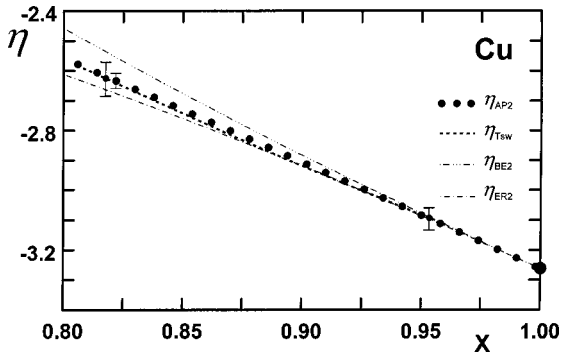

FIG. 16. APL scaling of the isothermal data p_T derived from the Hugoniot pressure p_H as discussed in the text in comparison with various isotherms derived from the ultrasonic data (K_0 and K_0') by the use of different EOS forms for Cu.

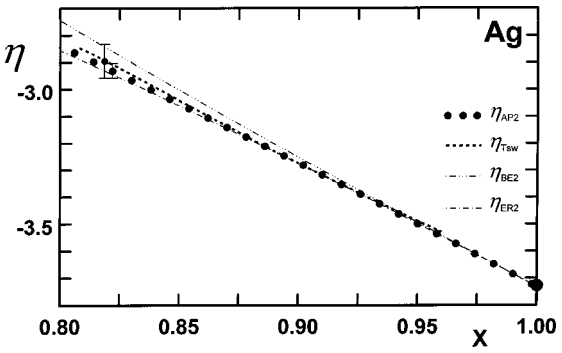

FIG. 17. APL scaling of the isothermal data p_T derived from the Hugoniot pressure p_H as discussed in the text in comparison with various isotherms derived from the ultrasonic data (K_0 and K_0') by the use of different EOS forms for Ag.

same curvature as AP2 but with a tendency to give too small values under strong compression. In fact, these deviations are similar to the deviations shown already in Figs. 10–12 with respect to the corresponding values for γ_{BS}.

Therefore, one may come to the conclusion that the evaluation of isotherms from the shock wave data with the present best form for $\gamma(v)$ leads to EOS data for Cu, Ag, and Au, which are best represented by the form AP2 when ultrasonic data are used for K_0 and K_0'.

5. Thermal Effects for Cu, Ag, and Au

As mentioned earlier, the most reliable data for these three elements are the data for V_0 and K_0 at ambient conditions as given in Table 1.

Temperature dependent data at ambient pressure for $V_0(T)$, $K_0(T)$, $K_0'(T)$, $\alpha_0(T)$, and $C_{p0}(T)$ from the literature[37,42–46,55–57] are then used, as discussed previously[5] for the case of Cu, to derive estimates for the best values and their uncertainties for K_0', θ_{D0}, γ_0, and $\Gamma_{\gamma 0}$ for ambient conditions. For a better fit of the $C_{p0}(T)$ data at lower temperatures, the previous pseudo-Debye model for the phonon internal energy $U_{\rm ph}(\tau)$ and for the corresponding specific heat capacity $C_v(\tau)$ with the scaled temperature $\tau = T/\theta_D$ was modified by the inclusion of two additional Einstein terms with the Einstein temperatures $\theta_{Ei} = f_i \cdot \theta_{D0}$, with best fitting values for f_1 and f_2, and with the constraints on the weights $g_1 = g_2 = .45$ and $g_D = 1 - g_1 - g_2 = 0.1$ in the quasiharmonic term

$$C_{\rm vqh} = 3R \cdot \Big(g_D \cdot \tau^3 \cdot (4 \cdot a \cdot g_D^{1/3} + \tau)/(a \cdot g_D^{1/3} + \tau)^4 + \sum_i g_i \cdot f_i^2/(2\tau \cdot \sinh(f_i/(2\tau)))^2 \Big). \quad (22)$$

For the parameter a, the low temperature value 0.372 was used in this case.[7] An overall fit for $C_{p0}(T)$ and the corresponding $\Gamma_{\alpha_0} = -(d \ln K_0(T)/dT)/\alpha_0(T)$ with the additional parameter A_a for the explicit anharmonic contribution has been presented recently[5] only for Cu; the results for Ag and Au are similar. Therefore only the corresponding parameter values are given in Table 1.

For the evaluation of the zero point energy, the ''average'' Debye temperature $\theta_{D\rm av} = \theta_{D0} \cdot 8 \cdot (a \cdot g_D + \Sigma_i f_i \cdot g_i/6)$ is used from the present second order modified Debye–Einstein fit (MoDE2), whereby θ_{D0} represents the low temperature limit of the commonly use temperature dependent Debye temperature according to the literature data given in Table 1, and $\theta_{D\rm av}$ from the present evaluation is given for comparison. The parameter sets from Table 1, together with the integrated form of Eq. (22), permit to derive from the room temperature data for Cu, Ag, and Au the best estimates for the static lattice pressure $p_{\rm sl}(v) = p_c(v) - p_{\rm zp}(v)$, whereby the pressure due to zero point motion is given by $p_{\rm zp}(v) = (9/8)R \cdot \gamma \cdot \theta_{D\rm av}$ and the corresponding values for the ''average'' Debye temperatures are given in Table 1. With all the uncertainties in γ and $p_H(v)$, the best fits of $p_{\rm sl}(v)$ are given by the previously discussed second order form AP2 Eq. (13) with very small values for $c_{2\rm sl}$. The values for the (secondary) parameters $V_{\rm sl0}, K_{\rm sl0}, K_{\rm sl0}', c_{2\rm sl}$ are shown in Table 3.

A comparison of experimental data with the fitted values for $V_0(T)$, $K_0(T)$, $K_0'(T)$, and $\gamma_0(T)$ corresponding to the

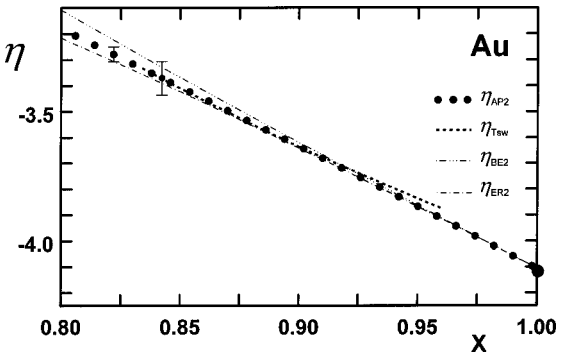

FIG. 18. APL scaling of the isothermal data p_T derived from the Hugoniot pressure p_H as discussed in the text in comparison with various isotherms derived from the ultrasonic data (K_0 and K_0') by the use of different EOS forms for Au.

TABLE 3. Secondary parameters $V_{\rm sl0}$, $K_{\rm sl0}$, $K_{\rm sl0}'$, and $C_{2\rm sl}$ for the static lattice with estimated uncertainties. $c_{2\rm sl} \neq 0$ represents thereby the (small) deviation from the simpler first order form AP1. Effective values K_{0-10}' and K_{0-100}' derived from fits of the best data for the T_R isotherm over different ranges in pressure by the use of effective AP2 forms are given for comparison with the K_0' values of Table 1.

	Cu	Ag	Au
$V_{\rm sl0}$/nm^3	0.011 613(1)	0.016 758(1)	0.016 736(1)
$K_{\rm sl0}$/GPa	146.4(7)	113.3(7)	183.6(7)
$K_{\rm sl0}'$	5.3(2)	5.9(3)	6.0(3)
$c_{2\rm sl}$	0.2(3)	0.8(4)	0.5(4)
	$K_{0\ \rm effective}'$ ($T = 300$ K)		
$K_{0\ 0-20\ \rm GPa}'$	5.48(15)	6.30(15)	6.40(15)
$K_{0\ 0-100\ \rm GPa}'$	5.45(15)	6.24(15)	6.34(15)
$K_{0\ 0-600\ \rm GPa}'$	5.40(15)	6.17(15)	6.27(15)
	$K_{0\ \rm effective}'$ ($T = 1500$ K)		
$K_{0\ 0-600\ \rm GPa}'$	6.20(15)	7.38(15)	7.33(15)

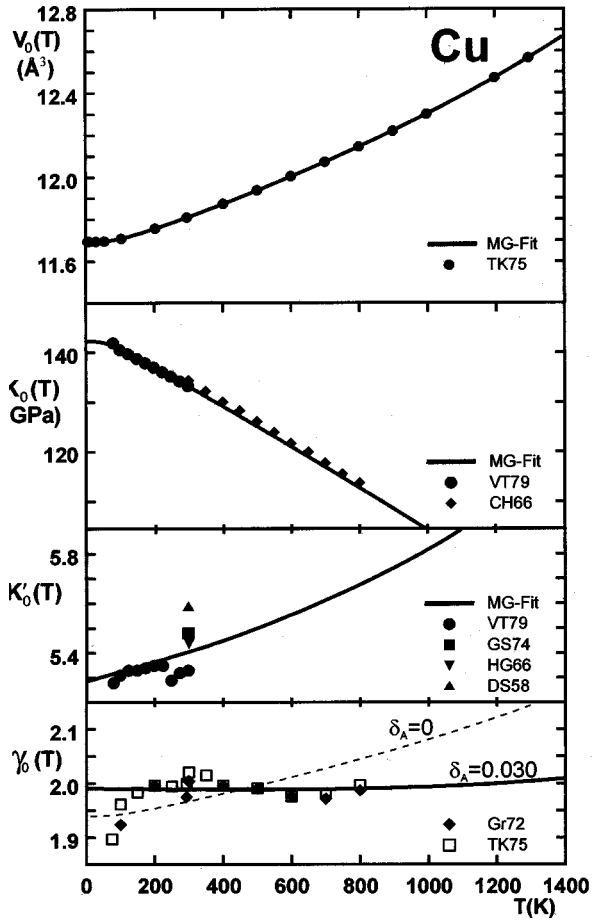

FIG. 19. Comparison of experimental data for $V_0(T)$, $K_0(T)$, $K_0'(T)$, and $\gamma_{\text{th}\,0}(T)$ from the literature (see Refs. 36, 38, 39, 42–44, 55–57) with the present best fits for Cu.

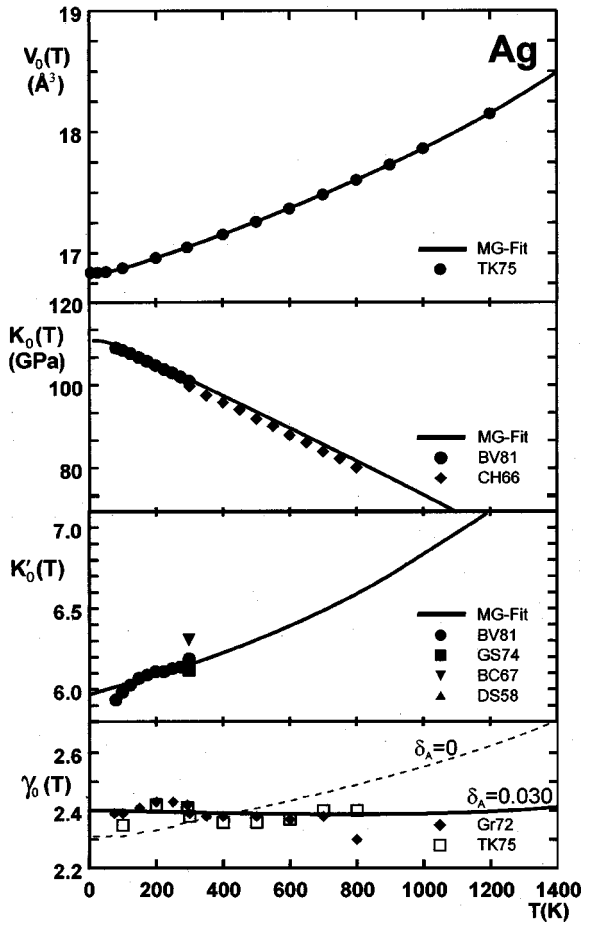

FIG. 20. Comparison of experimental data for $V_0(T)$, $K_0(T)$, $K_0'(T)$, and $\gamma_{\text{th}\,0}(T)$ from the literature (see Refs. 36, 41–43, 45, 55–57) with the present best fits for Ag.

parameter sets of Tables 1 and 2 is given in Figs. 19–21 for Cu, Ag, and Au, respectively. The special temperature dependence of $\gamma_0(T)$ at low temperatures ($\tau<1$) is related to differing mode Grüneisen parameters γ_i, which are represented by just one average Grüneisen parameter γ_θ in the Mie–Grüneisen approach. However, due to the small values of the thermal pressure at low temperatures, this difference can be neglected within the present experimental accuracy of EOS data. At higher temperatures ($\tau>1$), on the other hand, the best fit of $\gamma_0(T)$ is obtained with finite values for the anharmonicity parameter δ_A in Eq. (4). To remain within the Mie–Grüneisen approach, δ_A would have to be zero. However, to represent the curves for $V_0(T)$, $K_0(T)$, $K_0'(T)$ and $\gamma_0(T)$ within the given experimental uncertainties also at higher temperatures ($\tau>1$) finite values for $\delta_A\neq 0$ are needed as shown in Table 1. The theoretical background for the fitted curves justifies then extrapolations to lower and higher temperatures up to the corresponding melting curves. In fact, the residues between the experimental and fitted values for $V_0(T)$ amount to 200 ppm at the most, corresponding to pressure differences of less then 30 MPa near ambient pressure for temperatures below 1100 K. For Au this difference increases at 1200 K to 500 ppm or 80 MPa.

At this point one should note that only one isotherm can be represented precisely by the form AP2 if the thermal pressure is evaluated separately[5] as given here by the MoDE2 model with $\gamma(v)$ (using the parameters from Table 1). Nevertheless, the comparison for the 300 and 1500 K isotherms of Cu given in Fig. 22 illustrates that the differences are significant only at high temperatures, when the AP2 forms use the ''effective'' parameter for $K_0'(T)$ from Fig. 19 and the ''exact'' EOS form is based on the AP2 form for the static lattice with the parameters from Table 2 and the thermal pressure evaluated within the MoDE2 model using the parameters from Table 1 with $\gamma_{\text{sc}}(v)$ from Eq. (19) and the parameters v_d, A, B, and $\Delta\gamma_\infty$ from Table 2.

Using this background, detailed comparisons with previously published EOS data for the present high-pressure sensor materials are straightforward. Figure 23 presents the relative differences $\Delta p/p$ of different literature data[23,58–65,67,68,70,71] with respect to the present 300 K isotherm of Cu. Similar comparisons for Ag and Au are given in Figs. 24 and 25, respectively, on the basis of the available literature data.[23,46,58,61,65,66,72,73] Figure 26 compares the different literature data[66,46,74] and the effective AP2 form with the present ''exact'' form for the 1500 K isotherm of Au.

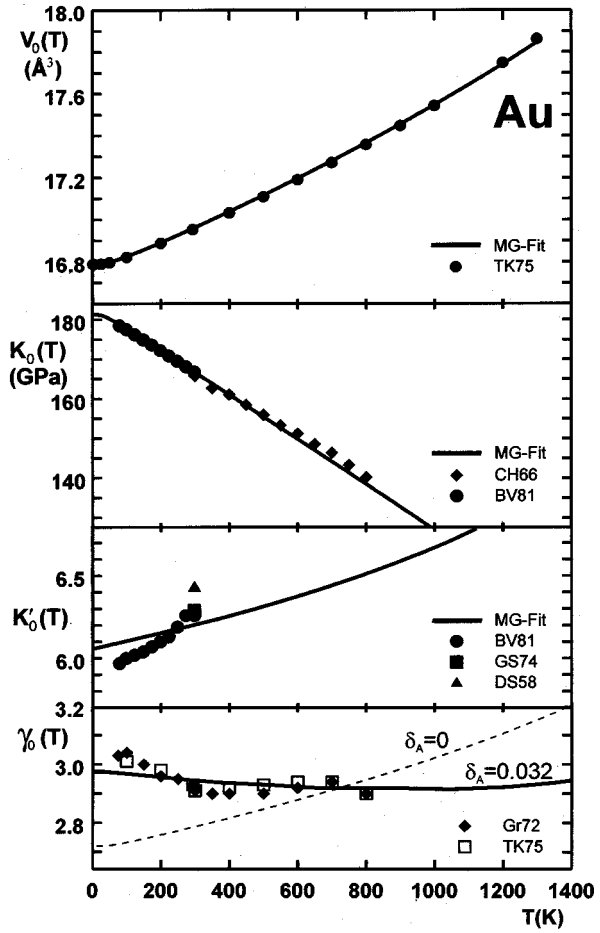

FIG. 21. Comparison of experimental data for $V_0(T)$, $K_0(T)$, $K_0'(T)$, and $\gamma_{th\,0}(T)$ from the literature (see Refs. 36, 38, 39, 42, 43, 45, 55–57) with the present best fits for Au.

6. Discussion of EOS Data for Cu, Ag, and Au

When the best fitted AP2 forms for the 300 K isotherms of Cu, Ag, and Au are used as baselines for the relative differences $\Delta p/p$ with respect to the experimental and theoretical data (refer to Figs. 23–25, respectively), one can notice several characteristic features:

(1) Most of the ''experimental'' data, representing in fact ''reduced'' shock wave data, show a positive curvature with large positive deviations $\Delta p/p$ at moderate pressures (below 10–80 GPa) and rather constant (negative) deviations at high pressure. The positive deviations (larger pressures) for the reduced shock wave data at moderate pressures can be traced back to the earlier observation that the (linear) extrapolation of u_s-u_p shock wave data into the region below the Hugoniot elastic limit result, in most cases, in extrapolated K_{H0} values, which are larger than the corresponding ultrasonic values and therefore lead to positive deviations of $\Delta p/p$ in this region. Accordingly, the K'_{H0} values are slightly smaller than the ultrasonic values (see also Table 1) to give a better fit of the u_s-u_p data with the erroneous K_{H0} value. This effect is most pronounced for the AIP handbook data[61] for Cu and Au and less pronounced for the corresponding data for Ag but again clearly visible for the later data[65] in Fig. 24,

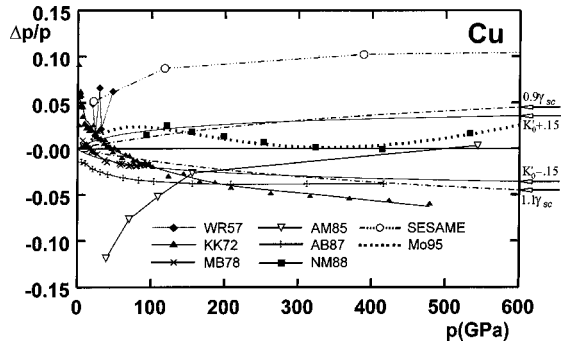

FIG. 23. Relative deviations $\Delta p/p$ of different literature data (see Refs. 23, 61, 63–65, 68, 70) from the present AP2 form for the 300 K isotherm of Cu. Modifications of the present best fit p_{AP2} according to a possible error in K_0' of ± 0.15 are indicated by two thin lines. Possible errors in the evaluation of the shock wave data by γ values, which are 10% too large or too small, are given by the dash-dotted curves.

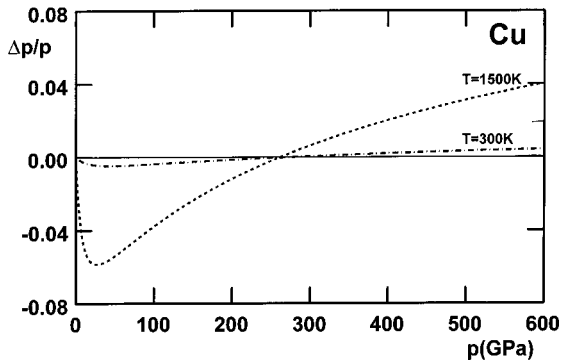

FIG. 22. Relative deviations $\Delta p/p$ of best fitted AP2 isotherms for Cu at 300 K and 1500 K based on the ''effective'' values $K_0'(T)$ for the range 0–600 K given in Table 3 with respect to ''exact'' isotherms based on an AP2 form for the static lattice pressure and the additional thermal pressure corrections.

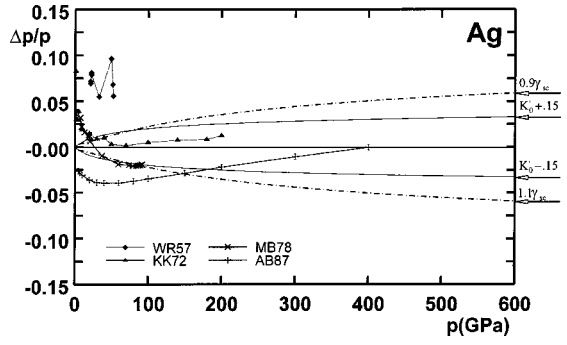

FIG. 24. Relative deviations $\Delta p/p$ of different literature data (see Refs. 23, 58, 61, 65) from the present AP2 form for the 300 K isotherm of Ag. Modifications of the present best fit p_{AP2} according to a possible error in K_0' of ± 0.15 are indicated by two thin lines. Possible errors in the evaluation of the shock wave data by γ values, which are 10% too large or too small, are given by the dash-dotted curves.

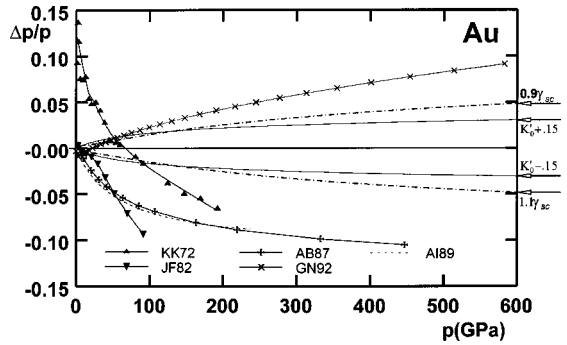

FIG. 25. Relative deviations $\Delta p/p$ of different literature data (see Refs. 23, 46, 61, 66, 73) from the present AP2 form for the 300 K isotherm of Au. Modifications of the present best fit p_{AP2} according to a possible error in K_0' of ± 0.15 are indicated by two thin lines. Possible errors in the evaluation of the shock wave data by γ values, which are 10% too large or too small, are given by the dash-dotted curves.

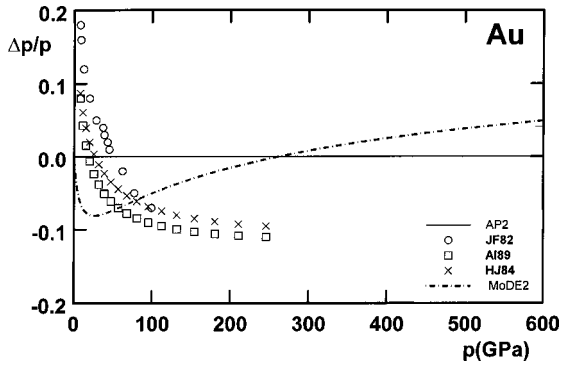

FIG. 26. Relative deviations $\Delta p/p$ of different literature data (Refs. 46, 66, 74) from the present AP2 form for the 1500 K isotherm of Au.

where the difference for the higher pressure data[23] becomes indeed very small.

Similarly, the difference with respect to the most recent theoretical data[68] for Cu in Fig. 23 becomes rather small in the 200–500 GPa range. The SESAME data[70] on the other hand show an almost constant 10% deviation in this pressure range.

For Au in Fig. 25, one can notice for the reduced shock wave data[23] at the highest pressure a large negative deviation but about the same positive deviation for the more recent data[73] based on modern total energy calculations. One can see also, that an earlier attempt[66] to evaluate both ultrasonic and shock wave data together lead primarily to a shift of the corresponding $\Delta p/p$ data to lower values with respect to the original evaluation.[61] A better fit with respect to the initial K_{T0} value was obtained in this way, however, with rather large deviations around 100 GPa.

(2) Whereas the uncertainty in the extrapolated K_{H0} values explains the deviations at low pressures, the uncertainties in $\gamma(v)$ needed in the reduction of the shock wave data can explain most of the differences at higher pressures. A $\pm 10\%$ uncertainty in γ is illustrated in Figs. 23–25 by the dash–dotted lines representing the differences, which would be obtained from the same Hugoniot pressure data just by these uncertainties in the thermal corrections. Since the fiducial values γ_f at higher pressures are estimated with typical uncertainties of only 10%, one may conclude that the comparison of the Hugoniot pressures with the more accurate ultrasonic data at moderate pressures leads primarily to constraints on $\gamma(v)$ but not to very accurate values for the isothermal pressures.

(3) Instead of this decoupling between the Hugoniot pressure data p_H and the isothermal data p_T, very often in the past isothermal data p_T had been used with the same kind of Slater form to couple p_T to $\gamma(v)$. In this way, a self-consistent procedure was used to evaluate p_T from p_H. However, this procedure depends on the assumption that this γ_{GS} is the correct form and thus introduces an additional uncertainty in the evaluation of p_T data.

(4) With these uncertainties of the reduced shock wave data in mind, one can see that the shock wave data possibly justify a reduction of the ''best'' K_0' value by 0.1 for Cu in Fig. 23 and no modification for Ag in Fig. 24. For Au in Fig. 25, there is the conflict between the reduced shock wave data and the theoretical data. The reduced shock wave data alone may justify a reduction of K_0' by up to 0.3 corresponding to 5%, but such a reduction would be in contrast to the ultrasonic data and more so with respect to the theoretical data.[73]

(5) Similarly, one can notice in Fig. 26 differences $\Delta p/p$ of $+18\%$ at low pressures and -10% at high pressure for the 1500 K isotherms of Au given in the literature[46,66,74] with respect to the present best fit based on an AP2 form for the static lattice and detailed modeling of the thermal pressure. The effective AP2 form for this 1500 K isotherm based on the same values of $V_0(T)$ and $K_0(T)$, but with the adjusted value for $K_0'(T)$ given in Table 3, shows even larger deviations at moderate pressures (<50 GPa), but minor deviations in the range from 50 to 150 GPa. However, it is not clear whether this improvement is significant or represents only an artifact.

(6) One may notice that the set of reduced shock wave data,[62] which was used to calibrate the ruby luminescence line shift with x-ray diffraction on Cu and Ag, shows here in both cases a negative difference of about 2% at 50 GPa with respect to the present AP2 estimate. This is about the same difference observed with different reference materials in later calibrations of the ruby scale.[71,75]

(7) While the use of the form AP2, Eq. (13), for the room temperature isotherms for Cu, Ag, and Au with the ultrasonic data for K_0 and K_0' is fully compatible with the reduced shock wave data, both the Birch BE2 and the Vinet ER2 forms lead to divergences at strong compression, not only in the isotherms but also in the forms for γ based on the Barton–Stacey form.

(8) The use of the complete thermodynamic model with an AP2 form for the static lattice pressure and a MoDE2 (modified Debye Einstein) model for the lattice contribution in the Mie–Grüneisen approximation with explicit anharmonic corrections results in isotherms p_{MG} also for elevated temperatures up to the melting curves. It is noted, that all these isotherms are also well represented by the AP2 form with

TABLE 4. Secondary parameters for Cu, Ag, and Au for the calculation of isotherms with the effective AP2 form of Eq. (13).

	Cu			Ag			Au		
T/K	$V_0(T)$/nm^3	$K_0(T)$/GPa	$K_0'(T)_{0-600\ \mathrm{GPa}}$	$V_0(T)$/nm^3	$K_0(T)$/GPa	$K_0'(T)_{0-600\ \mathrm{GPa}}$	$V_0(T)$/nm^3	$K_0(T)$/GPa	$K_0'(T)_{0-600\ \mathrm{GPa}}$
0	0.011 696 4	142.31	5.31	0.016 843 9	110.85	6.00	0.016 790 5	180.93	6.08
10	0.011 696 4	142.31	5.31	0.016 843 9	110.85	6.00	0.016 790 6	180.93	6.08
50	0.011 698 4	142.05	5.31	0.016 851 2	110.31	6.01	0.016 798 4	179.94	6.09
100	0.011 712 0	140.73	5.32	0.016 881 5	108.68	6.03	0.016 823 8	177.51	6.11
150	0.011 733 5	138.99	5.34	0.016 921 0	106.83	6.05	0.016 855 0	174.86	6.13
200	0.011 758 9	137.10	5.36	0.016 964 4	104.91	6.08	0.016 888 5	172.16	6.15
250	0.011 786 3	135.17	5.38	0.017 009 9	102.96	6.12	0.016 923 2	169.43	6.17
300	0.011 815 0	133.20	5.40	0.017 057 0	101.00	6.15	0.016 959 0	166.70	6.20
350	0.011 844 8	131.21	5.42	0.017 105 5	99.03	6.19	0.016 995 6	163.96	6.23
400	0.011 875 5	129.21	5.45	0.017 155 3	97.05	6.22	0.017 032 9	161.21	6.25
450	0.011 906 9	127.20	5.47	0.017 206 3	95.07	6.26	0.017 071 0	158.46	6.28
500	0.011 939 1	125.18	5.50	0.017 258 5	93.07	6.30	0.017 109 8	155.70	6.31

temperature dependent parameters $V_0(T)$, $K_0(T)$, and $K_0'(T)$, with systematic deviations of less than 0.25% in pressure in the case of Cu at room temperature and less than 0.35% for Ag and Au at pressures below 100 GPa. The values for p_{MG} are considered to be more reliable than the effective AP2 forms and some of the differences illustrated in Fig. 26 for the semiempirical curve[66] reflect just this difference between the present p_{MG} data and the effective AP2 forms.

(9) If the ultrasonic data for $K_0(T)$ are used in fits of effective AP2 forms to the calculated p_{MG} data for the pressure ranges from 0 to 20, 0 to 100, and 0 to 500 GPa, respectively, one obtains the ''effective'' $K_0'(T)$ values of Table 3 (lines 7–9), which indicate that any of the simple EOS forms for isotherms at finite temperatures give fits with differing K_0' (and K_0) values, depending on the range of pressures for the input data.

(10) For (future) pressure measurements in the 500 GPa range with the ambition to obtain an accuracy of better than 1% in pressure, the complete p_{MG} forms will have to be used, especially at elevated temperatures. It would appear to be interesting now to compare the present EOS data for Cu, Ag, and Au in x-ray measurements with hydrostatic media in an extended $p-T$ range up to the melting curves to obtain consistent EOS pairs for both p and T measurement just by the use of x-ray diffraction.[76,77]

(11) For a practical use of the present EOS data, Table 4 provides the input data for $V_0(T)$, $K_0(T)$, and $K_0'(T)$ for Cu, Ag, and Au. Intermediate values can be produced with a cubic spline to also obtain the values for the representation of any isotherm by an effective AP2 form, optimized for the pressure range up to 500 GPa. For temperatures above 500 K, the accuracy of this approximation decreases as illustrated in Fig. 22. For the best accuracy at higher temperatures the complete Mie–Grüneisen representation of the isotherms should be used with the parameters given in Tables 2 and 3. A website, www.EOSdata.de, is planned which allows one to calculate $p=p(V,T)$ or $V=V(p,T)$ for Cu, Ag and Au from the present input data (as given in Table 1).

The transfer of EOS data for solid phases of the elements in digital form to this website would be gratefully acknowledged with due reference to their origin to be used for the extension of this database.

7. References

[1] S. Eliezer, A. Ghatak, H. Hora, and E. Teller, *An Introduction to Equations of State: Theory and Applications* (Cambridge University Press, Cambridge, 1986). [It should be noted that the form Eq. (6) for the Hugoniot pressure given in this paper on p. 210 [Eq. (15.52)] includes a misprint in its denominator, where *A* must be replaced by *B*.]
[2] G. Falk, *Physik—Zahl und Realität* (Birkhäuser Verlag, Basel, 1990).
[3] G. Carrington, *Basic Thermodynamics* (Oxford University Press, Oxford, 1994).
[4] J. M. Besson and W. B. Holzapfel, ''Pressure Determination,'' p. 47, and ''Techniques for the Study of Physical Properties,'' p. 57, in *High Pressure Techniques and Physics*, edited by W. B. Holzapfel and N. Isaacs (Oxford University Press, Oxford, 1997).
[5] W. B. Holzapfel, High Press. Res. **16**, 81 (1998).
[6] V. N. Zharkov and V. A. Kalinin, *Equations of State for Solids at High Pressure and Temperatures* (Consultants Bureau, New York, 1971).
[7] W. B. Holzapfel, J. Phys. Chem. Solids **55**, 711 (1994).
[8] K. V. Khishchenko, C. E. Fortov, and I. V. Lomonosov, *High-Temperature, High-Pressure Equation of State for Polymer Materials*, pp. 103–106 in: *Shock Compression of Condensed Matter*, edited by Schmidt, Dandekar, and Forbes (The American Institute of Physics, Woodbury, 1997).
[9] J. Xie, St. de Gironcoli, St. Baroni, and M. Scheffler, Phys. Rev. B **59**, 965 (1999).
[10] D. C. Wallace, *Thermodynamics of Crystals* (Wiley, New York, 1972).
[11] W. B. Holzapfel (unpublished).
[12] G. A. Gschneidner, Jr., Solid State. Phys. **16**, 275 (1964).
[13] V. P. Kopyshev, Sov. Phys.-Dokl. **10**, 338 (1965).
[14] M. Ross, Rep. Prog. Phys. **48**, 1 (85).
[15] R. M. Moore, K. H. Warren, D. A. Young, and G. B. Zimmermann, Phys. Fluids **31**, 3059 (1988).
[16] M. Ross and D. A. Young, Ann. Rev. Phys. Chem. **44**, 61 (1993).
[17] Yu. V. Petrov, High Press. Res. **11**, 313 (1994).
[18] S. Visvanathan, Phys. Rev. **81**, 626 (1951).
[19] S. L. Thompson and H. S. Lauson, Sandia Corporation Livermore Report SC-RR-710714 (1972) (unpublished).
[20] P. R. Couchman and C. L. Reynolds, Jr., J. Phys. Chem. Solids **36**, 834 (1975).
[21] B. I. Bennett, J. D. Johnson, G. I. Kerley, and G. T. Rood, Los Alamos Scientific Laboratory, Report LA-7130 (1978) (unpublished).
[22] B. K. Godwal, S. K. Sikka, and R. Chidambaram, Phys. Rep. **102**, 121, (1983).

[23] L. V. Al'tshuler, S. E. Brusnikin, and E. A. Kuz'menkov, J. Appl. Mech. Tech. Phys. **28**, 129 (1987).
[24] A. V. Bushman, I. V. Lomonosov, and V. E. Fortov, Sov. Tech. Rev. B. Therm. Phys. **5**, 1 (1993).
[25] A. V. Bushman, I. V. Lomonosov, V. E. Fortov, K. V. Khishchenko, M. V. Zhernokletov, and Yu. N. Sutulov, JETP **82**, 895 (1996).
[26] K. V. Khishchenko, I. V. Lomonosov, and V. E. Fortov, High Temp. -High Press. **30**, 373 (1998).
[27] V. E. Fortov, K. V. Khishchenko, P. R. Levashov, and I. V. Lomonosov, Nucl. Instrum. Methods Phys. Res. A **415**, 604 (1998).
[28] M. Van Thiel, ''Compendium of Shock Wave Data,'' Lawrence Livermore Laboratory, Report UCRL 50108 (1977).
[29] M. H. Rice, R. G. McQueen, and J. M. Walsh, *Compression of Solids by Shock Waves*, in: Solid State Physics, Vol. 6, edited by F. Seitz and D. Turnbull (Academic, New York, 1958).
[30] L. V. Al'tshuler, K. K. Krupnikov, B. N. Ledenev, V. I. Zhuchikhin, and M. I. Brazhnik, Sov. Phys. JETP **34**, 606 (1958).
[31] J.-P. Poirier, *Introduction of the Physics of the Earth's Interior* (Cambridge University Press, Cambridge, 1991).
[32] F. E. Prieto and C. Renero, Phys. Rev. B **49**, 15498 (1994).
[33] Th. J. Ahrens and R. Jeanloz, J. Geophys. Res. **92**, 10363 (1987).
[34] P. Vinet, J. Ferrante, J. R. Smith, and J. H. Rose, J. Phys.: Condens. Matter **19**, L467 (1986).
[35] W. B. Holzapfel, Europhys. Lett. **16**, 67 (1991).
[36] W. B. Daniels and C. S. Smith, Phys. Rev. **111**, 713 (1958).
[37] I. E. Leksina and S. I. Novikova, Sov. Phys. Solid State **5**, 798 (1963).
[38] Y. Hiki and A. Granato, Phys. Rev. **144**, 411 (1966).
[39] Y. A. Chang and L. Himmel, J. Appl. Phys. **37**, 3567 (1966).
[40] B. Golding, S. C. Moss, and B. L. Averbach, Phys. Rev. **158**, 637 (1967).
[41] G. R. Barsch and Z. P. Chang, Phys. Status Solidi **19**, 139 (1967).
[42] G. Simmon and H. Wang, *Single Crystal Elastic Constants and Calculated Aggregate Properties: A Handbook* (MIT Press, Cambridge, MA, 1971).
[43] M. W. Guinan and D. J. Steinberg, J. Phys. Chem. Solids **35**, 1501 (1974).
[44] P. Van't Klooster, N. J. Trappeniers, and S. N. Biswas, Physica B **97**, 65 (1979).
[45] S. N. Biswas, P. Van't Klooster, and N. J. Trappeniers, Physica B **103**, 235 (1981).
[46] O. L. Anderson, D. G. Isaak, and S. Yamamoto, J. Appl. Phys. **65**, 1534 (1989).
[47] D. A. Young, *Phase Diagrams of the Elements* (University California Press, Berkeley, 1991).
[48] J. C. Slater, *Introduction to Chemical Physics* (McGraw-Hill, New York, 1939).
[49] J. S. Dugdale and D. K. C. McDonald, Phys. Rev. **89**, 832 (1953).
[50] V. Y. Vashchenko and V. N. Zubarev, Sov. Phys. Solid State **5**, 653 (1963).
[51] R. D. Irvine and F. D. Stacey, Phys. Earth Planet. Inter. **11**, 157 (1975).
[52] M. A. Barton and F. D. Stacey, Phys. Earth Planet. Inter. **39**, 167 (1985).
[53] F. D. Stacey, Phys. Earth Planet. Inter. **89**, 219 (1995).
[54] R. W. G. Wyckhoff, *Crystal Structures* (Interscience, New York, 1963).
[55] Y. S. Touloukian, R. K. Kirby, R. E. Taylor, and P. D. Desai, *Thermophysical Properties of Matter, Thermal Expansion, Metallic Elements and Alloys* (IFI/Plenum, New York, 1975), Vol. 12.
[56] *AIP Handbook*, 3rd ed., edited by D. E. Gray (McGraw-Hill, New York, 1972).
[57] Y. S. Touloukian and E. H. Buyco, *Thermophysical Properties of Matter, Specific Heat, Metallic Elements and Alloys* (IFI/Plenum, New York, 1970), Vol. 4.
[58] J. M. Walsh, M. H. Rice, R. G. McQueen, and F. L. Yarger, Phys. Rev. **108**, 196 (1957).
[59] L. V. Al'tshuler, A. A. Bakanova, and R. F. Trunin, Sov. Phys. JETP **15**, 65 (1962).
[60] R. F. Trunin, M. A. Podurets, B. N. Moiseev, G. V. Simakov, and L. B. Popov, Sov. Phys. JETP **29**, 630 (1969).
[61] R. N. Keeler and G. C. Kennedy, *American Institut of Physics Handbook*, 3rd ed., edited by D. E. Gray (McGraw-Hill, New York, 1972), p. 4938.
[62] A. C. Mitchell and W. J. Nellis, J. Appl. Phys. **52**, 3363 (1981).
[63] R. C. Albers, A. K. McMahan, and J. E. Miller, Phys. Rev. B **31**, 3435 (1985).
[64] W. J. Nellis, J. A. Moriarty, A. C. Mitchell, M. Ross, R. G. Dandrea, N. W. Ashcroft, N. C. Holmes, and G. R. Gathers, Phys. Rev. Lett. **60**, 1414 (1988).
[65] H. K. Mao, P. M. Bell, J. W. Shaner, and D. J. Steinberg, J. Appl. Phys. **49**, 3276 (1978).
[66] J. C. Jamieson, J. N. Fritz, and M. H. Manghnani, *High Pressure Research in Geophysics*, edited by S. Akimoto, and M. H. Manghnani (Center for Academic Publication, Tokyo, 1982), p. 27.
[67] A. C. Mitchell, W. J. Nellis, J. A. Moriarty, R. A. Heinle, N. C. Holmes, R. E. Tipton, and G. W. Repp, J. Appl. Phys. **69**, 2981 (1991).
[68] J. A. Moriarty, High Press. Res. **13**, 343 (1995).
[69] F. Birch, J. Geophys. Res. **83**, 1257 (1978).
[70] D. Young provided these data with permission from Lawrence Livermore Lab., 1999.
[71] H. K. Mao, J. Xu, and P. M. Bell, J. Geophys. Res. **91**, 4673 (1986).
[72] B. K. Godwal and R. Jeanloz, Phys. Rev. B **40**, 7501 (1989).
[73] B. K. Godwal, A. Ng, and R. Jeanloz, High Pressure Res. **10**, 7501 (1992).
[74] D. L. Heinz and R. Jeanloz, J. Appl. Phys. **55**, 885 (1984).
[75] C.-S. Zha, H.-K. Mao, and R. J. Hemley, Proc. Natl. Acad. Sci. U.S.A. **97**, 13494 (2000).
[76] Y. Zhao, R. B. von Dreele, D. J. Weidner, and D. Schiferl, High Press. Res. **15**, 369 (1997).
[77] Y. Zhao, R. B. Von Dreele, D. J. Weidner, and S. M. Stishov, J. Appl. Phys. **32**, 218 (1999).